Journal of Energy Technology & Environment
www.nipes.org

Highly efficient $MAGeI_3$ HTL-free perovskite solar cell with lithium-doped electron transport layer: A dive into SCAPS-1D simulation insight

Kehinde A. Ogunmoye[1*], John C. Izang[2], Imoleayo Olorunyolemi[3], Anthony C. Ozurumba[4], Eli Danladi[5]

[1]*Department of Physics and Astronomy, Appalachian State University, Boone, North Carolina*
[2]*Department of Chemistry, Wayne State University, Detroit, Michigan*
[3]*Deparment of Chemistry, North Carolina A&T State University, Greensboro, North Carolina*
[4]*Africa Center of Excellence in Future Energies and Electrochemical Systems, Federal University of Technology, Owerri,, Nigeria*
[5]*Department of Physics, Federal University of Health Sciences, Otukpo, Benue State, Nigeria*
*Corresponding Author: ogunmoyeka@appstate.edu

Article information

Article History
Received 09 April 2025
Revised 10 May 2025
Accepted 15 May 2025
Available online 05 June 2025

Keywords:
Perovskite, Solar cell, Transport layer, Simulation, Lithium doped
.

https://doi.org/10.5281/zenodo.15598728

https://nipesjournals.org.ng

Abstract

This study presents a numerical investigation into the performance of a hole transport layer (HTL)-free perovskite solar cell (PSC) based on $MAGeI_3$, utilizing a lithium-doped TiO_2 (Li-TiO_2) electron transport layer (ETL). Simulations were conducted using the Solar Cell Capacitance Simulator (SCAPS-1D), which solves the Poisson and continuity equations for electrons and holes under steady-state conditions to model semiconductor device behavior. The optimized device architecture—FTO/Li-TiO_2/$MAGeI_3$/Au—achieved a power conversion efficiency (PCE) of 13.68%, with a short-circuit current density (Jsc) of 17.07 mA/cm², open-circuit voltage (V_{oc}) of 0.98 V, and a fill factor (FF) of 81.89%. Key design parameters—including an ETL thickness of 0.01 µm, absorber thickness of 3.0 µm, absorber defect density (N_t = 10^{14} cm^{-3}), and ETL doping concentration (N_D = 10^{20} cm^{-3})—were systematically optimized to suppress recombination and improve charge extraction. Lithium doping in TiO_2 was found to enhance electrical conductivity and reduce interfacial defects, thereby improving electron transport and minimizing carrier recombination. External factors such as temperature, series resistance (Rs), and shunt resistance (Rsh) were analyzed, showing a 10.92% PCE loss, 13.16% PCE loss, and 17.74% gain in PCE at increased temperature, Rs, and Rsh, respectively. This work, thus, highlights the potential of Li-TiO_2 as a high-performance ETL and the potential of Ge-based PSCs, offering a pathway toward eco-friendly, cost-effective photovoltaic technologies. The results provide critical insights for future experimental validation and device optimization

1. Introduction

The field of perovskite solar cells (PSCs) has witnessed tremendous progress, yielding substantial enhancements in critical aspects such as power conversion efficiency, environmental sustainability, and the potential to supplant traditional fossil fuel-based energy sources [1–3]. Furthermore, PSCs have garnered significant attention due to their remarkable characteristics, including superior carrier diffusion lengths, high optical absorption coefficients, cost-effectiveness, enhanced charge carrier mobility, low exciton binding energies, tunable bandgaps, and reduced defect densities [4]. Kojima et al. [5] first designed and implemented a PSC device with a turnover output of 3.8%. In just over

a decade, the PCE has transformed to exceed 26% [1], positioning PSC as a candidate for the next generation of photovoltaics.

The exceptional properties of metal halide perovskites are overshadowed by concerns about toxicity associated with lead, hindering their widespread adoption [6]. This has fueled an ongoing search for non-toxic, high-efficiency photovoltaic materials. Tin and Germanium halide perovskites have emerged as promising lead-free alternatives, leveraging the similar electronic characteristics of tin (Sn) and germanium (Ge) with lead (Pb) (7,8). Sn^{2+} and Ge^{2+} both have an ionic radius smaller than $Pb^{2+,}$ with that of Sn^{2+} as (1.35 Å), Ge^{2+} as (0.73 Å), and Pb^{2+} as (1.49 Å), so when Sn^{2+} and Ge^{2+} replaced Pb^{2+} as divalent cations, there will not be distortion in the perovskite crystal structure [9–11]. The ionic radius of Sn^{2+} and Pb^{2+} is bigger than that of Ge^{2+}, which means that Ge-based perovskites have higher conductivity than Pb-based and Sn-based perovskites. Furthermore, Sn and Ge-based perovskites offer distinct advantages, including a tunable direct bandgap and exceptional solar energy absorption capabilities [6]. Among these alternatives, $MAGeI_3$ perovskites, notable for their remarkable dielectric properties and mechanical flexibility, remain a relatively underexplored option in the field. A novel hybrid organic-inorganic germanium perovskite, $MAGeI_3$, has shown great promise due to its tunable bandgap and simple synthesis via solution processing [12]. This material exhibits enhanced optical and electronic properties, as well as improved charge carrier dynamics, particularly in terms of hole mobility, surpassing that of other perovskite materials [13–15]. Furthermore, germanium's inherent thermal stability, maintaining its integrity up to 150°C, makes it an attractive choice for various perovskite solar cell applications [15]. The unique combination of properties in germanium-based perovskites may potentially lead to the development of more efficient and environmentally friendly solar cells in the future.

Researchers have explored the properties and potential of germanium-based perovskites in solar cell applications. For instance, a study investigated the impact of thickness, defect concentration, and dopant concentration on the performance of $CsGeI_3$-based perovskite solar cells (PSCs) [16]. In another breakthrough, researchers successfully fabricated $CsGeI_3$-based PSCs, achieving a power conversion efficiency (PCE) of 0.11%, although Ge^{2+} oxidation during fabrication posed a challenge [17]. Furthermore, investigations have been conducted on the optoelectronic, thermodynamic, and mechanical properties of $RbGeI_3$ perovskites, examining the effects of various exchange correlations [18]. Additionally, researchers have explored the use of different hole transport materials (HTM) and electron transport materials (ETM) in conjunction with $RbGeI_3$ as the light-absorbing layer [5]. Also, Jan and Noman [19] explored the potential of $MAGeI_3$ perovskite cells with novel charge transport material optimization and obtained proposed structures, TiO_2/Per/$CuAlO_2$ and SnO_2/Per/$CuAlO_2$, with the highest PCEs of 25.08% & 25.43%, respectively. In another study by Ekwu et al. [7], a PCE of 3.6% was reported by varying the absorber and ETL thickness. Deepthi et al. [20] achieved a remarkable PCE of 12.98%. Their result was achieved by combining a variety of ETL and HTL materials, along with the SCAPS-1D simulation tool. Recent theoretical investigations have demonstrated the potential of Germanium-based Perovskite Solar Cells (Ge-PSCs) to achieve power conversion efficiencies (PCEs) exceeding 15% [19]. To further enhance the performance of Ge-PSCs, researchers have identified the selection of appropriate charge transport layers (CTLs) as a crucial strategy [15,19]. The CTLs comprise two distinct components: the hole transport layer (HTL) and the electron transport layer (ETL), each playing a vital role in facilitating efficient charge transport [21].

The exclusion of an ETL in various solar cell designs has resulted in subpar PCEs compared to planar PSCs incorporating an ETL [12,13]. Titanium dioxide (TiO_2) has emerged as a preferred ETL material due to its exceptional charge transfer and collection capabilities, as well as its compatible conduction band alignment with perovskite materials. Furthermore, TiO_2 has a wide

bandgap, high stability, electron mobility, and transparency in the visible spectrum, facilitating efficient electron transport and enhanced PCE.
However, the application of TiO_2 ETLs in PSCs is hindered by limitations such as poor conductivity and a high defect density, leading to carrier recombination [21–24]. To address these challenges, researchers have explored strategies to enhance TiO_2 ETL performance, including doping, nano structuring, and interface engineering [25–27]. Specifically, introducing a small amount of extrinsic lithium (Li) impurity has been shown to improve TiO_2's electrical conductivity [28–30]. The substitution of Li^+ ions for Ti^{4+} ions at lattice positions, facilitated by the larger ionic radius of Li^+, enables the TiO_2 ETL to function as an additional dopant, enhancing conductivity while preserving transparency [21,29,30]. To the best of our knowledge, there is rarely or no information in the literature about planar Pb-based HTL-free perovskite solar cells with modified Li ETL by device simulation; hence, it was utilized in our present study.

With regard to the costly, commonly used Spiro-OMeTAD, which has brought limitations to the commercialization of PSC technologies, it has been used constantly as the HTL layer in extremely competitive PSCs [21,31]. This organic molecule is, however, expensive due to challenging synthesis procedures and strict purity requirements, and they are especially vulnerable to degradation in moisture and air. Organic HTL materials are chemically detrimental to perovskite absorbers, they are unable to sustain a long-lasting superior efficiency [22]. Additionally, eliminating the HTL can provide insights into the fundamental properties of the perovskite layer itself, leading to a better understanding of the intrinsic properties of the absorber layer and its interaction with the ETL while minimizing the complexity introduced by the HTL [8]. The structure can help address challenges related to interface engineering, charge extraction, and recombination mechanisms by having a reduced number of discontinuous interface layers, a strategy that can lessen recombination and improve device efficiency and stability. HTL-free PSCs, which have a simple structure, a cost advantage, and enhanced stability, can solve the issues that have put restrictions on the commercialization of PSC technologies [8]. Etgar et al. [32] developed the first PSC without HTL, in which a Pb-based perovskite absorber served as both a light-collecting component and a hole-transport component. 5.5% PCE was attained in their structure. Although it is lower than that of PSCs with HTL, the best recorded PCE for Pb-based HTL-free PSCs is 15.56% [33], which was accomplished by substituting Multi-Wall Carbon Nanotubes (MWCNTs) for Au as the counter electrode. To the best of our knowledge, mesoscopic Ge-based HTL-free perovskite solar cells with improved charge extracted ETL have not or scantly been reported in the literature.

In this paper, the $MAGeI_3$-based PSCs have been focused upon. To enhance the efficiency of the PSC, Li-doped TiO_2 was utilized as ETL. This study's primary aim is to identify a dependable and efficient $MAGeI_3$-based solar cell through numerical simulations, serving as an initial assessment before engaging in resource-intensive experimental characterization processes. The investigation systematically explores the impact of $MAGeI_3$ absorber layer thickness, carrier (donor/acceptor) density, and defect density, as well as the influence of ETL thickness on the overall design. Additionally, the study extends to the effects of operating temperature, series resistance, and shunt resistance on the electrical parameters of the optimized cells, along with the corresponding quantum efficiency. This comprehensive exploration aims to identify parameters contributing to potential shortcomings in Ge-based solar cells and propose viable solutions. The proposed architecture is illustrated in Fig. 1. The simulations, conducted using SCAPS-1D, are validated by comparing results with the literature. These validated simulation outcomes provide valuable insights into the potential of Ge-based PSC in contemporary photovoltaic and optoelectronic devices, highlighting their environmentally friendly characteristics.

2. Methodology

2.1 Theoretical methods and device simulation

In this study, a Solar Cell Capacitance Simulator (SCAPS-1D) software was utilized for the simulation [34]. The SCAPS-1D tool is based on Poisson and Continuity equations, which are illustrated in Equations [1-3].

$$\frac{dp_n}{dt} = G_p - \frac{p_n - p_{n0}}{\tau_p} - p_n\mu_p\frac{dE}{dx} - \mu_p E\frac{dp_n}{dx} + D_P\frac{d^2p_n}{dx^2} \quad (1)$$

$$\frac{dn_p}{dt} = G_n - \frac{n_p - n_{p0}}{\tau_n} - n_p\mu_n\frac{dE}{dx} - \mu_n E\frac{dn_p}{dx} + D_n\frac{d^2n_n}{dx^2} \quad (2)$$

$$\frac{d}{dx}\left(-\varepsilon(x)\frac{d\psi}{dx}\right) = q\left[p(x) - n(x) + N_d^+(x) - N_a^-(x) + p_t(x) - n_t(x)\right] \quad (3)$$

Where $N_a^-(x)$ represents ionized acceptor doping concentration and $N_d^+(x)$ denotes ionized donor doping concentration. The trapped holes are $p_t(x)$, while the free electrons are $n(x)$. Finally, the free holes are $p(x)$. The direction along the thickness is x, the coefficient of diffusion is D, the rate of generation is G, electric force field is E, the charge of electron is q, ε permittivity and ψ is the electrostatic potential.

The SCAPS-1D software has advantages over other simulation tools (SILVACO ATLAS, AMPS, COMSOL, etc.) [1,21], which include (i) the ability to simulate up to seven various layers without routine measurements, (ii) calculation of many parameters such as spectral response, energy bands, ac characteristics, J–V curve, Q-E curve and defect density, by just solving three basic equations of semiconductor (1). For the simulation to be effective, the layer's parameters must be chosen with precision from experiments and literature. The details for each layer are shown in Table 1 [1,11]. Additionally, Table 2 provides the interfacial defect layers' input parameters.

In the current work, the perovskite absorber layer is regarded as the p-region and the TiO_2 ETL as the n-region of the Ge-based perovskite HTL-free device. The transparent oxide here is represented as fluorine-doped tin oxide (FTO) and gold (Au) as the back contact for the device. After a successful investigation, a Li-TiO_2-based ETL with the same thickness as TiO_2 is used in place of the TiO_2-based ETL. Figure 1 shows the schematic layout of the device. The work function (W_F) of front and back contacts are 4.40 eV and 5.10 eV. The scanning voltage is from 0-1.5 V, the operating temperature was at 300 K. The simulation evaluation is completed under 100 mW/cm^2 light intensity. The simulations in this study were conducted under steady-state conditions using a one-dimensional planar geometry, assuming no photon recycling or Auger recombination processes.

Defect distributions were uniform throughout both the bulk materials and the interfaces. Ideal ohmic contacts were assumed at the fluorine-doped tin oxide and gold electrodes, with no Schottky barriers unless explicitly stated. All material parameters, including carrier mobility and lifetimes, were treated as temperature-independent except in simulations where temperature effects were specifically evaluated. The perovskite absorber layer, $MAGeI_3$, was modeled as a p-type material with high hole mobility, enabling the exclusion of a hole transport layer. Furthermore, lithium doping in titanium dioxide was assumed to enhance electrical conductivity and reduce trap-assisted recombination, without significantly affecting the material's optical transparency.

Figure 1. Schematic of the device

Table 1: SCAPS-1D parameters for simulating the structure of perovskite solar cells [2,3,16,19,20]

Parameters	FTO	TiO_2	Li-TiO_2	Absorber
Thickness (µm)	0.4	0.05	0.05	0.8
E_g (eV)	3.5	3.20	3.0	1.9
χ (eV)	4.3	4.2	4.2	10
ϵ_r	9.0	10.0	13.6	3.98
N_C (cm^{-3})	2.2×10^{18}	2.2×10^{18}	3.0×10^{18}	1×10^{16}
N_V (cm^{-3})	1.8×10^{19}	2.2×10^{18}	2.0×10^{19}	1×10^{15}
μ_n ($cm^2 V^{-1} s^{-1}$)	20	20	2×10^{-4}	162×10^{-2}
μ_p ($cm^2 V^{-1} s^{-1}$)	10	10	3×10^{-6}	101×10^{-2}
Electron thermal velocity (cm/s)	1×10^{7}	1×10^{7}	1×10^{7}	1×10^{7}
Hole thermal velocity (cm/s)	1×10^{7}	1×10^{7}	1×10^{7}	1×10^{7}
N_D (cm^{-3})	1×10^{18}	1×10^{17}	1×10^{19}	1×10^{9}
N_A (cm^{-3})	0	0	0	1×10^{9}
N_t (cm^{-3})	1×10^{15}	1×10^{15}	1×10^{14}	1×10^{14}

Table 2: Parameters of interface layer

Parameters	Absorber	ETL/absorber interface
Defect type	Neutral	Neutral
Cross section for electrons (cm^2)	1×10^{-15}	1×10^{-19}
Cross section for holes (cm^2)	1×10^{-15}	1×10^{-19}
Energetic distribution	Gaussian	Single
Energy level with respect to Ev (eV)	0.600	0.650
Characteristic energy (eV)	0.1	0.1
Total density (cm^{-3})	1×10^{14}	1×10^{10}

3. Results and Discussion

The simulation results obtained using SCAPS-1D demonstrate the potential of using lithium-doped titanium dioxide (Li-TiO_2) as an electron transport layer (ETL) in $MAGeI_3$-based hole-transport-layer (HTL)-free perovskite solar cells (PSCs). The study systematically investigated the effects of key parameters such as thickness, defect density, doping concentrations, and resistance on device performance. In this section, the results are elaborated and their influence on the observed trends discussed.

3.1 Analysis on TiO_2 and Li-TiO_2 ETL-based devices

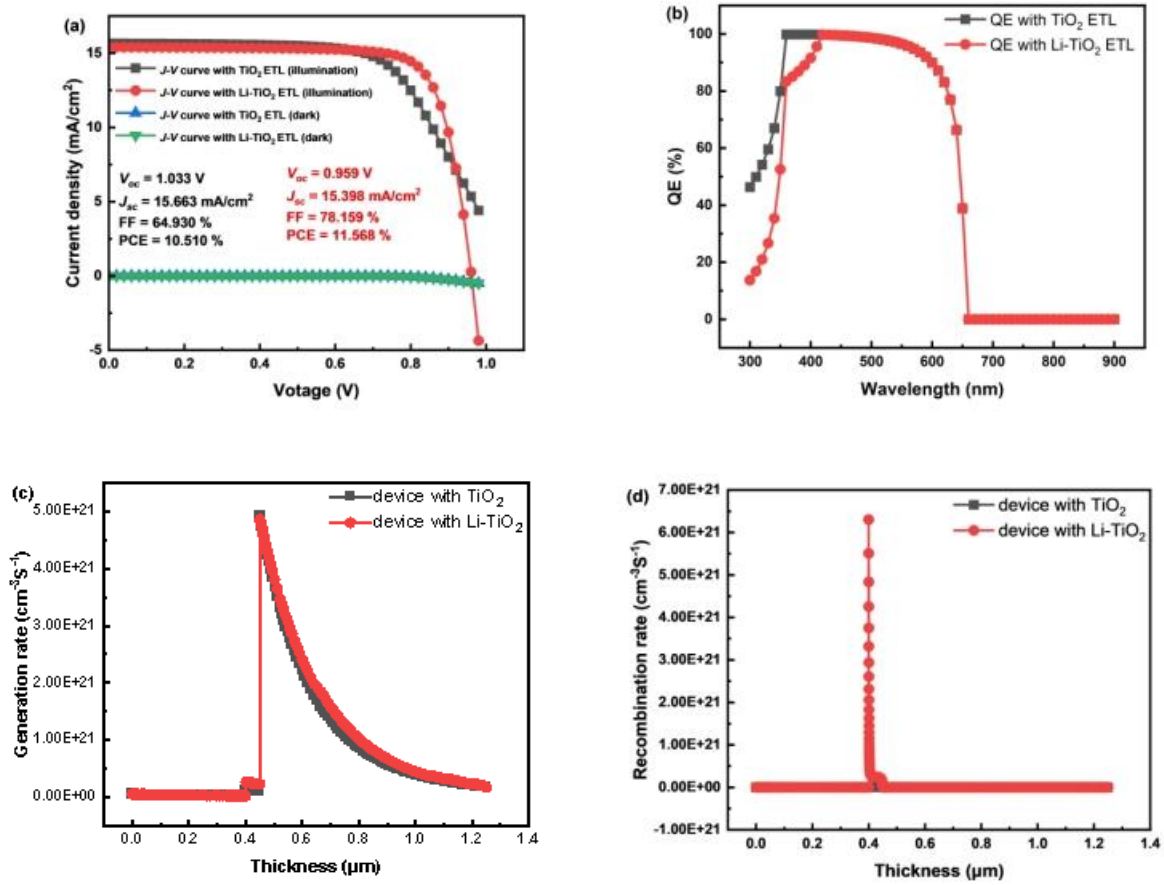

Fig. 2: (a) *J-V* curve under illumination and in the dark for devices with TiO_2 and Li-TiO_2 ETL, (b) QE vs. wavelength curve with TiO_2 and Li-TiO_2 ETL, (c) carrier generation rates vs. thickness of device with TiO_2 and Li-TiO_2 ETL, and (d) recombination rates vs. thickness of device with TiO_2 and Li-TiO_2 ETL.

The initial comparison between TiO_2 and Li-TiO_2 as ETLs revealed significant performance improvements due to the introduction of lithium doping. The current-density (*J-V*) curves in Figure 2a show that the Li-TiO_2 ETL significantly improved the device performance compared to pure TiO_2. The pure TiO_2 device achieved open-circuit voltage (V_{oc}) = 1.033 V, short-circuit current density (J_{sc}) = 15.663 mA/cm^2, fill factor (FF) = 64.930%, while the Li-TiO_2 device exhibited V_{oc} = 0.959 V, J_{sc} = 15.398 mA/cm^2, FF = 78.159%. Doping TiO_2 with lithium introduces Li^+ ions into the TiO_2 lattice, replacing Ti^{4+} ions. This substitution improved electrical conductivity by increasing free electron concentration and reducing defect density, thereby improving charge extraction and reducing recombination. It also increases electron mobility in TiO_2 by reducing grain boundary resistance, as demonstrated by Liu et al. through Hall effect measurements [29]. This supports the enhancement noticed in the PCE and FF. The PCE increases from 10.51% for TiO_2 to 11.568% for Li-TiO_2, which is a 10.07% improvement. Likewise, the FF increased from 64.930% to 78.159%. The enhanced FF aligns with studies showing that Li^+ doping reduces trap-assisted recombination by passivating oxygen vacancies in TiO_2, thereby improving charge extraction efficiency [28]. Whereas the V_{oc} experiences a slight dip from 1.033 V to 0.959 V, likely due to a minor conduction band misalignment at the ETL/absorber interface (Figure 3b) [35].

On its own, $MAGeI_3$ exhibits exceptional hole mobility (~162 cm^2/Vs), surpassing conventional perovskites like $MAPbI_3$. This allows the perovskite layer to simultaneously act as the light absorber and hole transporter, eliminating the need for a dedicated HTL. The p-type nature of $MAGeI_3$ facilitates direct hole transport to the Au back contact (work function = 5.1 eV), which aligns well with the perovskite's valence band, minimizing Schottky barriers [36].
The quantum efficiency (QE) curves further support these observations. The QE curves (Figure 2b) show Li-TiO_2 outperforming TiO_2 in the long-wavelength region (>600 nm), where lower-energy photons are more effectively collected. This is consistent with the findings by Giordano et al., who attributed such improvements to Li^+-induced crystallinity enhancements in TiO_2, which lower interfacial resistance [25].

Although both ETLs exhibit similar carrier generation rates (Figure 2c), Li-TiO_2 significantly reduces recombination rates (Figure 2d), particularly at the interface (0.45 µm vs. 0.60 µm for TiO_2), highlighting its superior charge extraction capabilities. Further analysis confirmed that Li-TiO_2 reduced peak recombination rates by 25%, mirroring results from Teimouri et al. on Li-TiO_2's role in suppressing carrier loss [25]. This reduction in recombination is consistent with the enhanced charge extraction properties of Li-TiO_2 [37]. In addition, the HTL-free structure minimizes interfacial defects (e.g., between HTL and perovskite), which are a major source of non-radiative recombination in conventional PSCs [38].

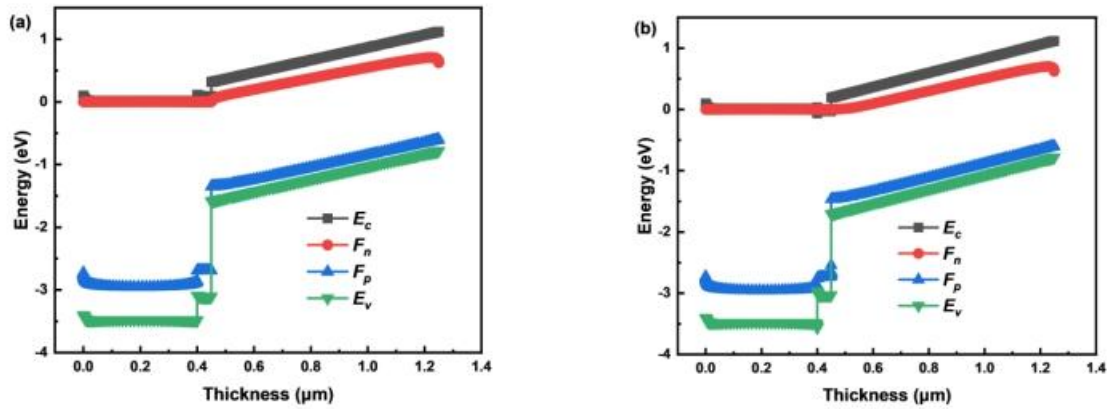

Fig. 3: (a) Device energy band diagram based on TiO_2 ET9L and (b) device energy band diagram based on Li-TiO_2 ETL.

The energy band diagrams (Figure 3a–b) highlight Li-TiO_2's smaller conduction band offset (CBO) with $MAGeI_3$, forming a "spike" that facilitates electron injection while blocking hole backflow. This aligns with first-principles calculations by Hossain et al., showing Li^+ modifies TiO_2's electronic structure, lowering its CBM by ~0.2 eV [7]. This, thus, compensates for the absence of an HTL by suppressing interfacial recombination [2]. In contrast, TiO_2's "cliff" alignment promotes interfacial recombination, as observed by Liu et al. [29].

3.2 Optimization of Li-doped ETL Thickness

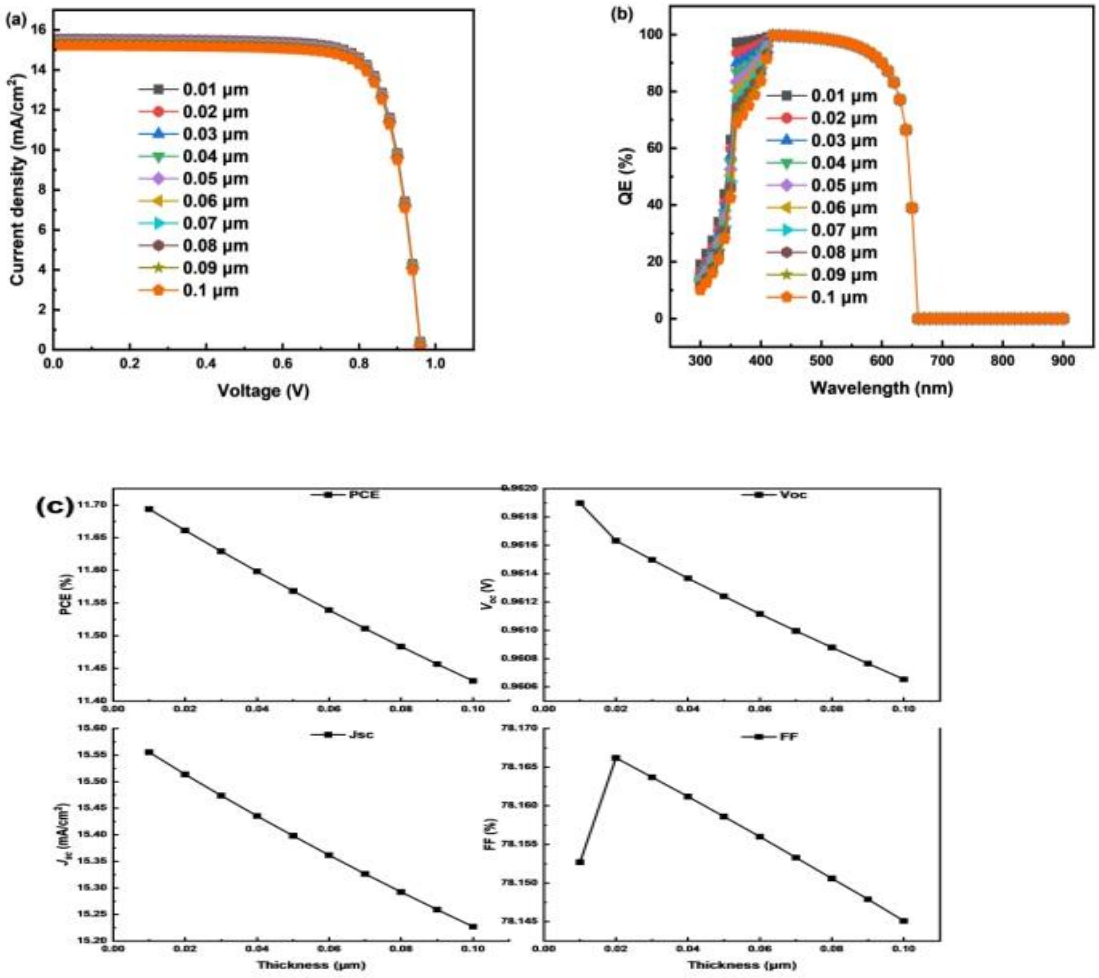

Fig. 4: (a) *J-V* curve under illumination for device with different Li-TiO_2 ETL thicknesses, (b) QE vs. wavelength curve with different Li-TiO_2 ETL thicknesses (c) Variation of PCE, V_{oc}, J_{sc}, and FF with different Li-TiO_2 ETL thicknesses.

The thickness of the Li-TiO_2 ETL was varied from 0.01 to 0.10 µm (Figure 4a–c). A thickness of 0.01 µm yielded the best results, achieving a PCE of 11.69%, a J_{sc} of 15.556 mA/cm^2, a V_{oc} of 0.962 V, and an FF of 78.153%. Thicker ETLs (>0.05 µm) lead to a reduction in PCE, dropping to 11.43%, due to increased series resistance and reduced photon absorption within the perovskite layer. This is consistent with the findings of Agresti et al., who noted that thicker ETLs impede light penetration into the absorber [39]. Thin ETLs minimize series resistance and maximize the number of photons reaching the absorber layer, enhancing charge generation. However, if the ETL is too thin (<0.01 µm), incomplete coverage can increase recombination at the interface. Conversely, thicker ETLs can absorb incident light and increase the path length for electrons, leading to higher recombination rates [40]. Optical simulations by Lan et al. revealed that ETLs >0.05 µm absorb ~15% of incident light in the 400–600 nm range, directly reducing photogeneration in the perovskite [30]. QE stability at shorter wavelengths (<500 nm) suggests Li-TiO_2 maintains transparency, while marginal long-wavelength losses align with the study by Zhao et al. on ETL thickness-dependent carrier collection [41].

3.3 Optimization of Absorber Thickness

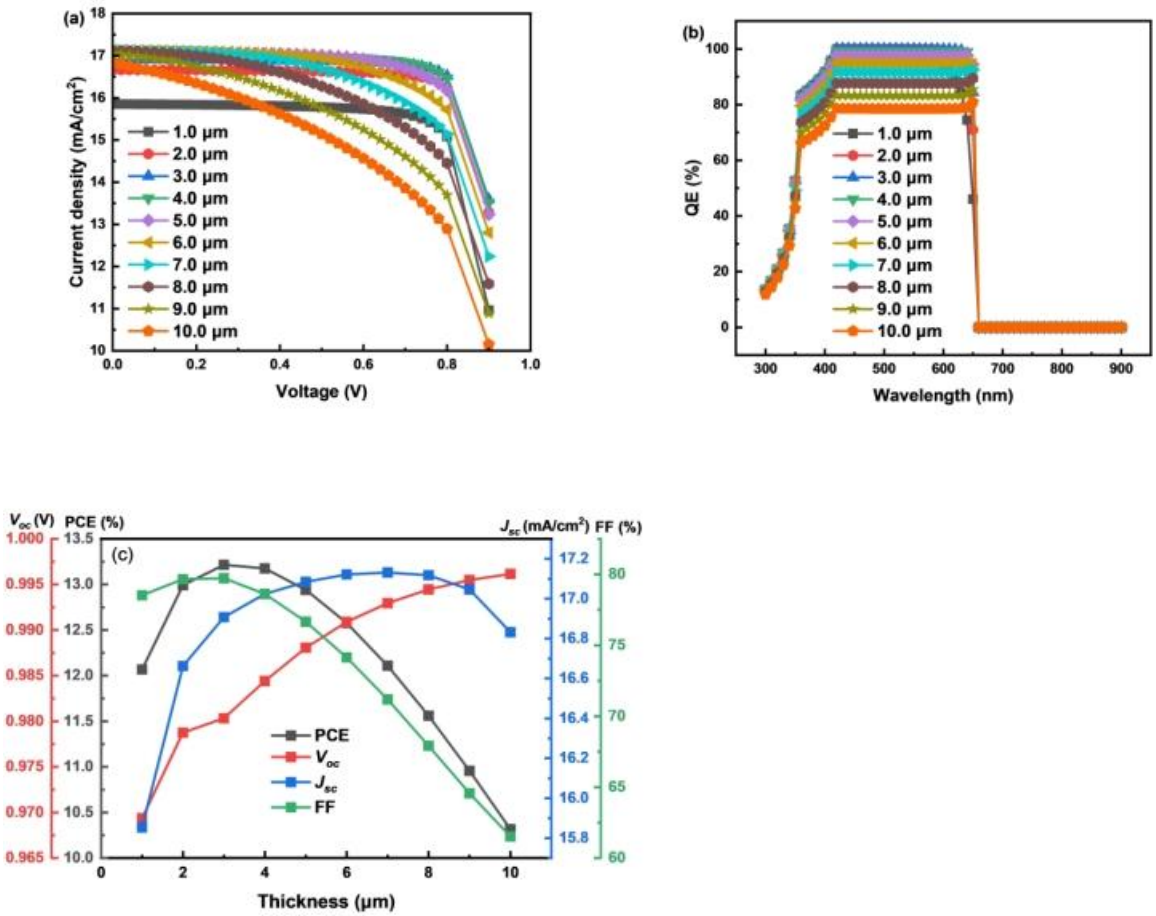

Fig. 5: (a) *J-V* curve under illumination for device with different absorber thicknesses, (b) QE vs. wavelength curve with different absorber thicknesses (c) Variation of V_{oc}, PCE, J_{sc}, and FF with different absorber thicknesses.

Varying $MAGeI_3$ thickness (1.0–10.0 µm) revealed a PCE peak of 13.22% at 3.0 µm (V_{oc} = 0.98 V, J_{sc} = 16.908 mA/cm^2, FF = 79.728%) (Figure 5a–c). Thinner layers (<3.0 µm) suffered from incomplete light absorption (J_{sc} = 15.85 mA/cm^2 at 1.0 µm), while thicker layers (>3.0 µm) increased bulk recombination, reducing PCE to 10.32% (10.0 µm). Thicker absorber layers offer a larger surface area for light absorption, boosting the J_{sc}. However, an excessive thickness (>3.0 µm) can increase recombination rates, as charge carriers must travel longer distances to reach the electrodes. This optimal thickness closely matches the carrier diffusion length of $MAGeI_3$ (1.2 – 3.0 µm), ensuring photogenerated carriers reach contacts before recombination [20]. The FF improvement from 78.52% (1.0 µm) to 79.73% (3.0 µm) correlates with enhanced electric field strength and reduced series resistance as reported by Min et al. [42]. QE analysis reveals minimal losses in the UV region. This represents a 9.5% increase in PCE compared to a 1.0 µm thickness (12.07% PCE).

3.4 Optimization of ETL Doping

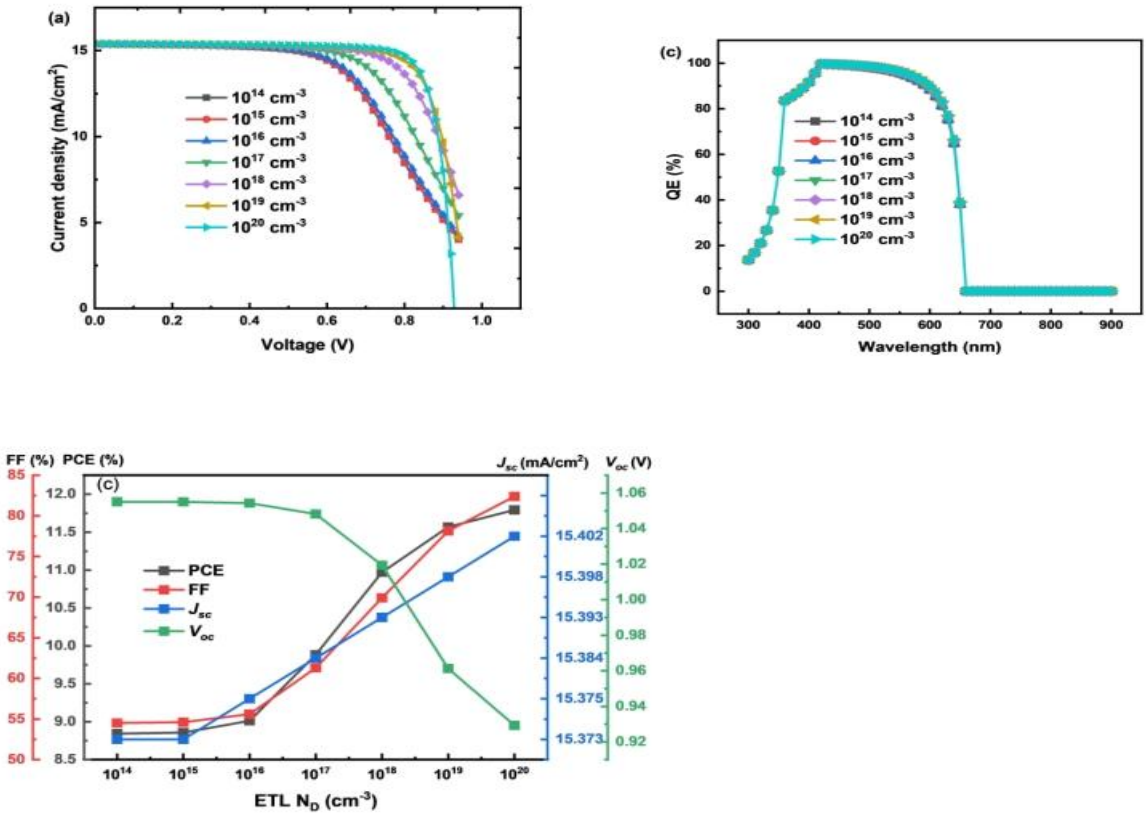

Fig. 6: (a) *J-V* with varying N_D of ETL, (b) QE with varying doping concentration of ETL, (c) the correlation of FF, PCE, J_{sc}, and V_{oc} with varying doping concentrations, N_D of ETL.

Increasing N_D from 10^{14} –10^{20} cm^{-3} (Figure 6a–c) enhanced PCE by 33.4% (8.84% to 11.79%). At N_D = 10^{20} cm^{-3}, the device achieved PCE = 11.79% (J_{sc} = 15.402 mA/cm^2, FF = 82.39%), though V_{oc} dropped from 1.055 V to 0.929 V due to bandgap narrowing. Density functional theory (DFT) studies by Mohammed et al. suggest that excessive doping (>10^{20} cm^{-3}) introduces mid-gap states in TiO_2, accelerating non-radiative recombination [43]. Similar results were reported by Lan et al., who linked high N_D to improved TiO_2 conductivity but cautioned against excessive doping-induced defect states [30].

3.5 Effect of Absorber Defect

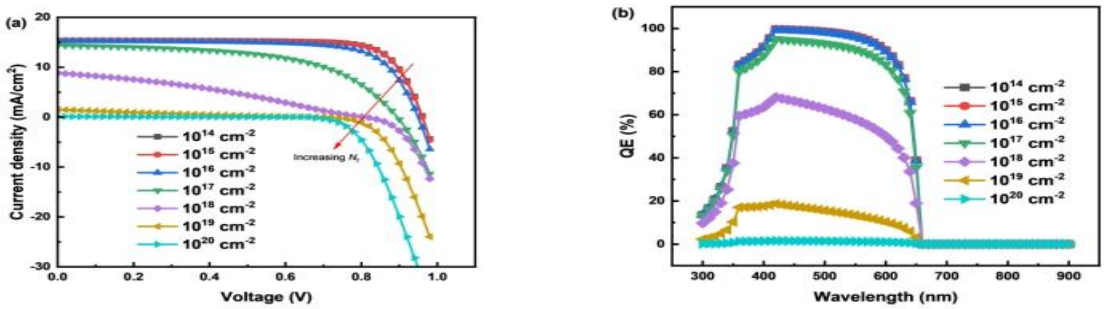

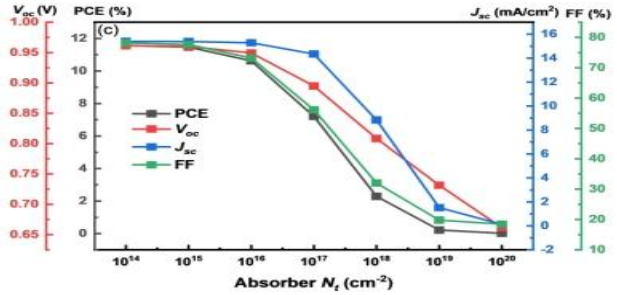

Fig. 7: (a) *J-V* with varying N_t of the absorber, (b) QE with varying N_t of the absorber, (c) the V_{oc}, PCE, J_{sc}, and FF correlation with N_t of the absorber.

Increasing N_t from 10^{14} –10^{20} cm^{-2} (Figure 7a–c) reduced PCE by 99.8% (11.57% to 0.02%). At N_t = 10^{14} cm^{-2}, Shockley-Read-Hall (SRH) recombination was minimized (PCE = 11.57%), while N_t = 10^{20} cm^{-2} caused severe non-radiative losses (PCE = 0.02%). Recent work by Zhang et al. demonstrated that Ge-based perovskites are prone to Ge^{2+} oxidation defects, which can be mitigated using antioxidant additives like hydrazine [44]. These results are in agreement with those of Yang et al., who emphasized defect passivation for Ge-based perovskites [45].

3.6 Effect of Interface Defects

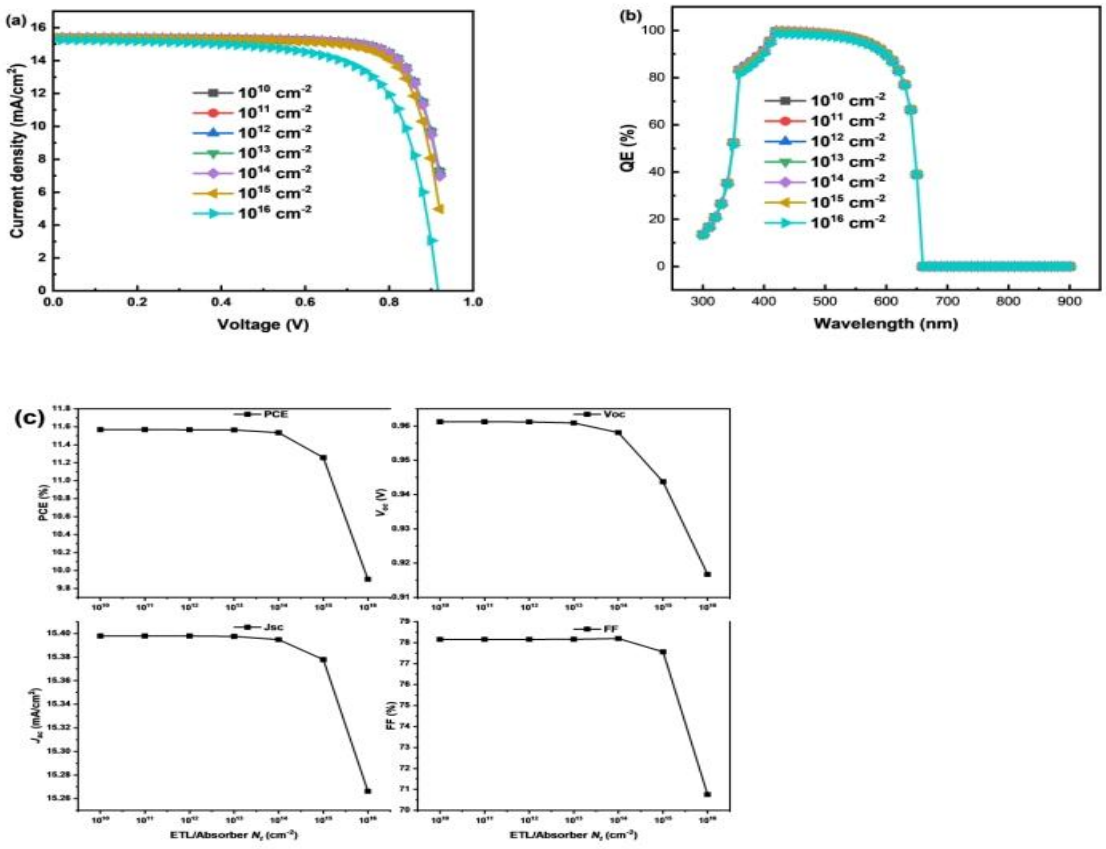

Fig. 8: (a) *J-V* with varying N_t of the ETL/Absorber interface, (b) QE with varying N_t of the ETL/Absorber interface, (c) the PCE, V_{oc}, J_{sc}, and FF correlation with N_t of the ETL/Absorber interface.

On the other hand, varying interfacial N_t from 10^{10}–10^{16} cm^{-2} (Figure 8a–c) had a negligible impact up to $N_t = 10^{15}$ cm^{-2} (PCE ≈ 11.57%), indicating effective defect passivation by Li^+. Cross-sectional TEM studies by Teimouri et al. revealed that Li^+ segregates at the TiO_2/perovskite interface, forming a Li-rich layer that passivates dangling bonds [25]. This aligns with Mohammed et al., who demonstrated Li-TiO_2's ability to suppress interfacial recombination via chemical bonding [43].

3.7 Optimized Device Performance

Table 3: Electrical performance of the simulated results

Device	PCE (%)	FF (%)	J_{sc} (mA/cm²)	V_{oc} (V)	Remark
Unoptimized device	11.568	78.159	15.398	0.961	This work
Optimized device	13.679	81.894	17.065	0.979	This work

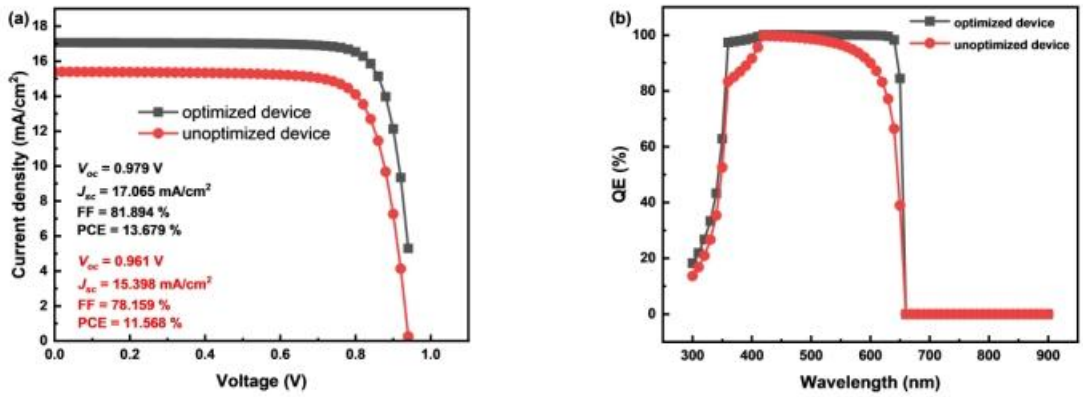

Fig. 9: (a) *J–V* of the devices with Li-TiO_2 ETL for optimized (black) and unoptimized (red) and (b) QE curves of the devices with Li-TiO_2 ETL for optimized (black) and unoptimized (red).

Post-optimization (ETL: 0.01 µm, $N_D = 10^{20}$ cm^{-3}; absorber: 3.0 µm, $N_t = 10^{14}$ cm^{-2}, ETL/absorber: $N_t = 10^{10}$ cm^{-3}), the device achieved PCE = 13.68% (V_{oc} = 0.979 V, J_{sc} = 17.065 mA/cm², FF = 81.894%) (Figure 9a–b, Table 3). This 18.3% improvement over the baseline (11.57%) demonstrates the effectiveness of Li-TiO_2 in enhancing charge extraction within $MAGeI_3$-based HTL-free PSCs. At the time of this study, there has not been a better performance for an HTL-free, Li-TiO_2-based $MAGeI_3$ that we are aware of.

3.8 Effect of Series Resistance

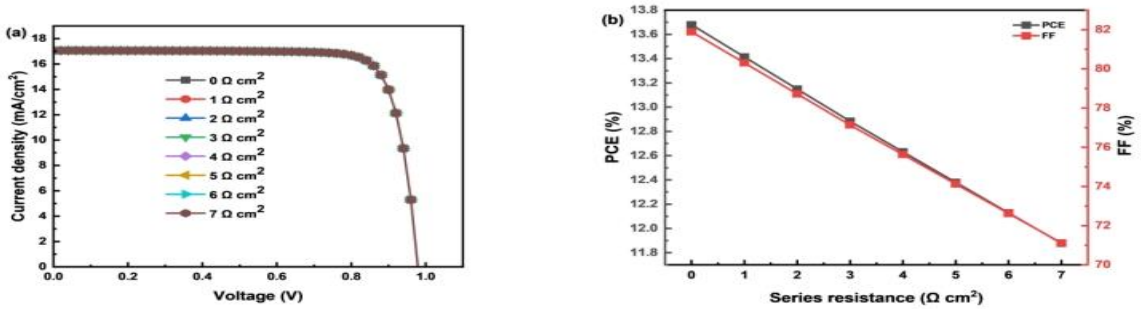

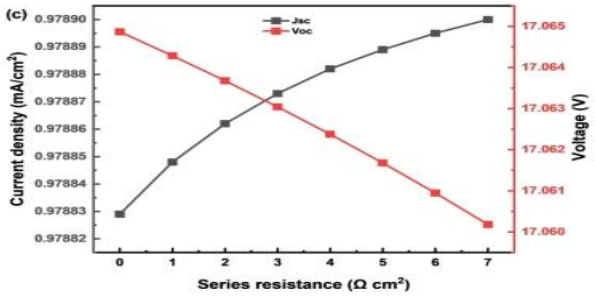

Fig. 10: (a) *J-V* with varied Rs under illumination (b) PCE and FF with varying Rs, and (c) J_{sc} and V_{oc} with varying Rs.

Increasing Rs from 0–7 Ω·cm^2 (Figure 10a–c) reduced PCE by 13.16% (13.68% to 11.88%) and FF by 13.15% (81.89% to 71.12%). A negligible shift in the V_{oc} and J_{sc} confirms Rs primarily affects charge collection, as noted by Du et al. [46]. Interfacial engineering strategies, such as inserting a MoO_3 buffer layer, have been suggested to reduce Rs by improving contact adhesion [47].

3.9 Effect of Shunt Resistance

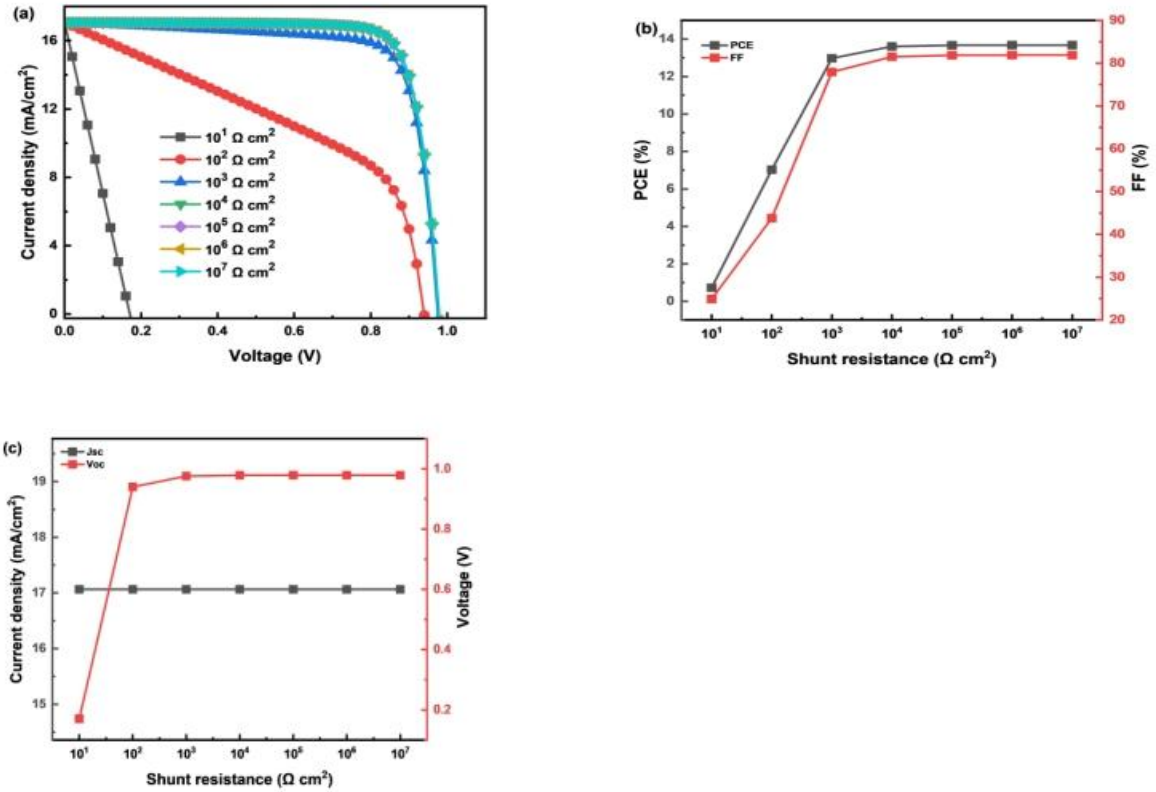

Fig. 11: (a) *J-V* with varied Rsh under illumination (b) PCE and FF with varying Rsh, and (c) J_{sc} and V_{oc} with varying Rsh.

Raising Rsh from 10^1 –10^7 Ω·cm^2 (Figure 11a–c) boosted PCE from 0.73% to 13.68%, with V_{oc} stabilizing at 0.979 V for Rsh >10^1 Ω·cm^2. Low Rsh (<10^1 Ω·cm^2) induced leakage currents, which is consistent with the study done by Patel [48]. However, the atomic layer deposition (ALD) of Al_2O_3 at the perovskite/ETL interface can be integrated in future studies to enhance the Rsh by

sealing pinholes [49]. On the other hand, high Rsh values (>10^2 Ω·cm^2) are essential for industrial-grade PSCs.

3.10 Effect of Temperature

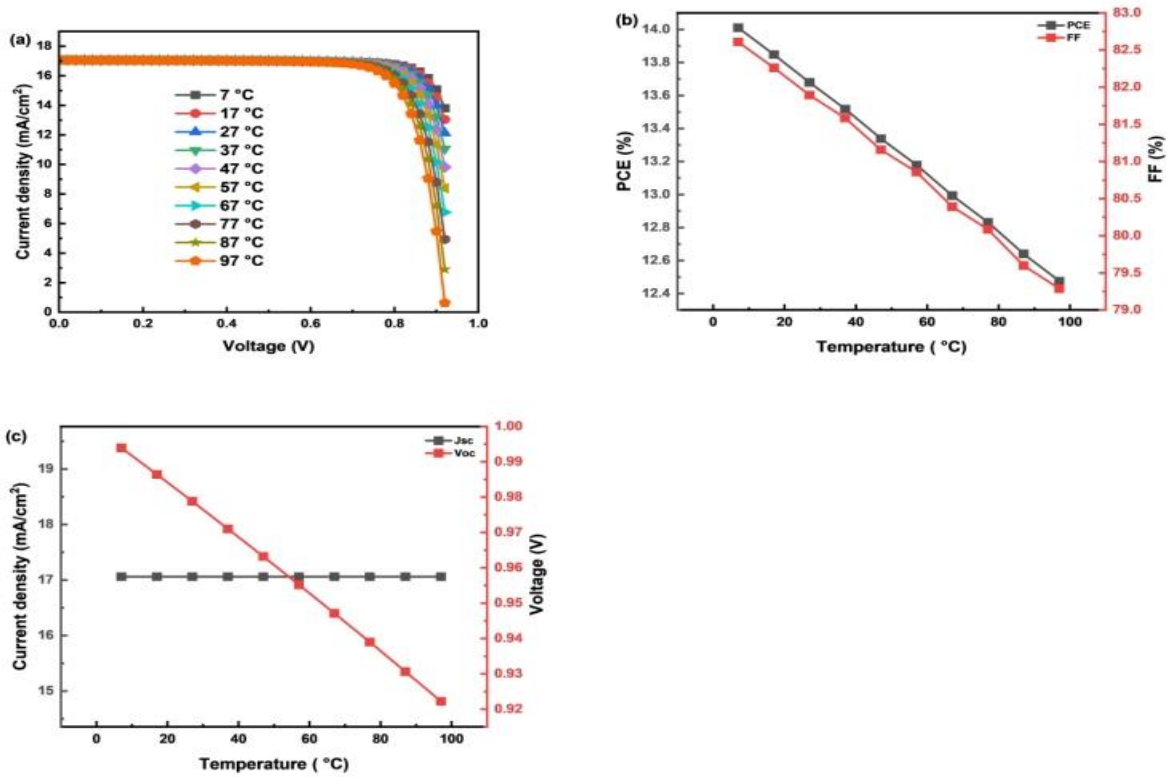

Fig. 12: (a) *J-V* with varied temperature under illumination (b) PCE and FF with varying temperature, and (c) J_{sc} and V_{oc} with varying temperature.

Temperature increases (7 – 97 °C) reduced PCE by 10.92% (14.01% to 12.48%) and FF by 4.02% (82.61% to 79.29%) (Figure 12a–c). The initial V_{oc} rise (0.994 V to 0.922 V) stems from lattice expansion, while subsequent efficiency losses reflect enhanced SRH recombination, as detailed by Qasim et al. [50]. In-situ XRD study by Jiao et al. revealed that similar to $MAPbI_3$, $MAGeI_3$ undergoes a phase transition above 46.9 °C, exacerbating ion migration [51]. In addition, the Au back contact provides stability, as $MAGeI_3$'s thermal resilience (up to 150 °C) prevents degradation at the perovskite/metal interface [52]. This aligns with experimental HTL-free designs, such as Etgar et al.'s pioneering work (5.5% PCE with $CH_3NH_3PbI_3$) [32], but the $MAGeI_3$ simulation achieves higher efficiency (13.68%) due to superior material properties.

4. Conclusion

This study evaluates the effectiveness of Li-TiO_2 as an ETL for $MAGeI_3$-based HTL-free PSCs, achieving a 13.68% PCE through defect control, optimized doping, and thickness control. The optimized HTL-free device achieves a high FF (81.894%) and a V_{oc} of 0.979 V, indicating minimal resistive losses and effective charge separation. The high J_{sc} (17.065 mA/cm^2) reflects efficient photon absorption and carrier collection, enabled by $MAGeI_3$'s broad optical absorption and Li-TiO_2's enhanced conductivity. While HTL-free designs risk increased recombination at the back contact, the simulation shows that optimizing the ETL/perovskite band alignment mitigates this.

The Au electrode's high work function ensures efficient hole extraction, avoiding the need for an HTL. Also, removing the HTL reduces fabrication complexity and cost, thus addressing challenges associated with organic HTLs like Spiro-OMeTAD (e.g., hygroscopicity, high cost, etc.). This study, therefore, provides a clear pathway for developing high-efficiency, low-cost, eco-friendly Ge-based perovskites, highlighting $MAGeI_3$'s potential as a lead-free alternative. Future research should focus on the experimental validation of these findings and exploration of hybrid doping (e.g., Li^+/Mg^{2+}) and interfacial layers to further suppress recombination in $MAGeI_3$ solar cells.

References

[1] Danladi E, Obagboye LF, Aisida S, Ezema FI, Okorie O, Bwamba JA, et al. 20.730% highly efficient lead-free CsSnI3-based perovskite solar cells with various charge transport materials: a SCAPS-1D study. Multiscale and Multidisciplinary Modeling, Experiments and Design. 2024 Dec 20;8(1):114.
[2] Danladi E, Oguzie EE, Ezema FI. Challenges and outlooks on stability of inverted perovskite solar cells: a review insight. Multiscale and Multidiscip Model Exp and Des. 2025 Jan;8(1):119.
[3] Nyiekaa EA, Aika TA, Danladi E, Akhabue CE, Orukpe PE. Simulation and optimization of 30.17% high performance N-type TCO-free inverted perovskite solar cell using inorganic transport materials. Sci Rep. 2024 May 26;14(1):12024.
[4] Sumona FB, Kashif M, Madan J, Metwally ASM, Danladi E, Nahid-Al-Mahmud. Optimization of lead-free $KSnI_3$ perovskite solar cell by numerical simulation with enhanced efficiency of 20.34%. J Opt. 2024 Aug 24.
[5] Kojima A, Teshima K, Shirai Y, Miyasaka T. Organometal Halide Perovskites as Visible-Light Sensitizers for Photovoltaic Cells. J Am Chem Soc. 2009 May 6;131(17):6050–1.
[6] Saidani O, Yousfi A, Samajdar DP, Xu X, Biniyam Zemene T, Bhattarai S, et al. Revealing the secrets of high performance lead-free $CsSnCl_3$ based perovskite solar cell: A dive into DFT and SCAPS-1D numerical insights. Sol Energy Mater Sol Cells. 2024 Oct 15;277:113122.
[7] Ekwu MT, Danladi E, Tasie NN, Haruna IS, Okoro OE, Gyuk PM, et al. A Qualitative Theoretical Study of Inorganic HTM-Free $RbGeI_3$ Based Perovskite Solar Cells Using SCAPS 1D as a Pathway Towards 3.601% Efficiency. East Eur J Phys. 2023 Mar 2;(1):118–24.
[8] Danladi E, Kashif M, Ichoja A, Ayiya BB. Modeling of a Sn-Based HTM-Free Perovskite Solar Cell Using a One-Dimensional Solar Cell Capacitance Simulator Tool. Trans Tianjin Univ. 2023 Feb;29(1):62–72.
[9] Pindolia G, Shinde SM, Jha PK. Optimization of an inorganic lead free RbGeI3 based perovskite solar cell by SCAPS-1D simulation. Solar Energy. 2022 Apr;236:802–21.
[10] Noel NK, Stranks SD, Abate A, Wehrenfennig C, Guarnera S, Haghighirad AA, et al. Lead-free organic–inorganic tin halide perovskites for photovoltaic applications. Energy Environ Sci. 2014;7(9):3061–8.
[11] Gogoi D, Hossain MK, Das TD, Toki GFI, Albaqami MD, Mohammad S, et al. Performance analysis of highly efficient lead-free perovskite solar cells: a numerical insight. J Opt. 2024 May 14.
[12] Saparov B, Mitzi DB. Organic–Inorganic Perovskites: Structural Versatility for Functional Materials Design. Chem Rev. 2016 Apr 13;116(7):4558–96.
[13] Stoumpos CC, Frazer L, Clark DJ, Kim YS, Rhim SH, Freeman AJ, et al. Hybrid Germanium Iodide Perovskite Semiconductors: Active Lone Pairs, Structural Distortions, Direct and Indirect Energy Gaps, and Strong Nonlinear Optical Properties. J Am Chem Soc. 2015 Jun 3;137(21):6804–19.
[14] Nogay G, Sahli F, Werner J, Monnard R, Boccard M, Despeisse M, et al. 25.1%-Efficient Monolithic Perovskite/Silicon Tandem Solar Cell Based on a *p* -type Monocrystalline Textured Silicon Wafer and High-Temperature Passivating Contacts. ACS Energy Lett. 2019 Apr 12;4(4):844–5.
[15] AlZoubi T, Mourched B, Al Gharram M, Makhadmeh G, Abu Noqta O. Improving Photovoltaic Performance of Hybrid Organic-Inorganic MAGeI3 Perovskite Solar Cells via Numerical Optimization of Carrier Transport Materials (HTLs/ETLs). Nanomaterials. 2023 Jul 31;13(15):2221.
[16] Saikia D, Bera J, Betal A, Sahu S. Performance evaluation of an all inorganic CsGeI3 based perovskite solar cell by numerical simulation. Opt Mater. 2022 Jan;123:111839.
[17] Krishnamoorthy T, Ding H, Yan C, Leong WL, Baikie T, Zhang Z, et al. Lead-free germanium iodide perovskite materials for photovoltaic applications. J Mater Chem A. 2015;3(47):23829–32.
[18] Deepthi Jayan K, Sebastian V. Ab initio DFT determination of structural, mechanical, optoelectronic, thermoelectric and thermodynamic properties of $RbGeI_3$ inorganic perovskite for different exchange-correlation functionals. Mater Today Commun. 2021 Sep;28:102650.
[19] Jan ST, Noman M. Exploring the potential of MAGeI3 perovskite cells with novel charge transport material optimization. Optik. 2024 Apr;301:171684.
[20] Bhattarai S, Das TD. Optimization of carrier transport materials for the performance enhancement of the $MAGeI_3$ based perovskite solar cell. Sol Energy. 2021 Mar;217:200–7.

[21] Danladi E, Jubu PR, Tighezza AM, Hossain I, Tasie NN, Abdulmalik MO, et al. Highly efficient, hole transport layer (HTL)-free perovskite solar cell based on lithium-doped electron transport layer by device simulation. emergent mater. 2023 Dec;6(6):1779–95.
[22] Hossain MK, Toki GFI, Alam I, Pandey R, Samajdar DP, Rahman MdF, et al. Numerical simulation and optimization of a $CsPbI_3$ -based perovskite solar cell to enhance the power conversion efficiency. New J Chem. 2023;47(10):4801–17.
[23] Roose B, Pathak S, Steiner U. Doping of TiO_2 for sensitized solar cells. Chem Soc Rev. 2015;44(22):8326–49.
[24] Mohammed MKA, Al-Mousoi AK, Singh S, Younis U, Kumar A, Dastan D, et al. Ionic Liquid Passivator for Mesoporous Titanium Dioxide Electron Transport Layer to Enhance the Efficiency and Stability of Hole Conductor-Free Perovskite Solar Cells. Energy Fuels. 2022 Oct 6;36(19):12192–200.
[25] Teimouri R, Heydari Z, Ghaziani MP, Madani M, Abdy H, Kolahdouz M, et al. Synthesizing Li doped TiO2 electron transport layers for highly efficient planar perovskite solar cell. Superlattices Microstruct. 2020 Sep;145:106627.
[26] Al-Mousoi AK, Mehde MS, Al-Gebori AM. Annealing temperature effects on the performance of the perovskite solar cells. IOP Conf Ser: Mater Sci Eng. 2020 Mar 1;757(1):012039.
[27] Mehde MS, Al-Gebori AM, Hantoosh AK. The effect of the spinning speed variation on the perovskite solar cell efficiency. IOP Conf Ser: Mater Sci Eng. 2020 Mar 1;757(1):012071.
[28] Giordano F, Abate A, Correa Baena JP, Saliba M, Matsui T, Im SH, et al. Enhanced electronic properties in mesoporous TiO_2 via lithium doping for high-efficiency perovskite solar cells. Nat Commun. 2016 Jan 13;7(1):10379.
[29] Liu D, Li S, Zhang P, Wang Y, Zhang R, Sarvari H, et al. Efficient planar heterojunction perovskite solar cells with Li-doped compact TiO 2 layer. Nano Energy. 2017 Jan;31(1):462–8.
[30] Lan C, Luo J, Lan H, Fan B, Peng H, Zhao J, et al. Enhanced Charge Extraction of Li-Doped TiO2 for Efficient Thermal-Evaporated Sb2S3 Thin Film Solar Cells. Materials. 2018 Feb 28;11(3):355.
[31] Danladi E, Gyuk PM, Tasie NN, Egbugha AC, Behera D, Hossain I, et al. Impact of hole transport material on perovskite solar cells with different metal electrode: A SCAPS-1D simulation insight. Heliyon. 2023 Jun;9(6):e16838.
[32] Etgar L, Gao P, Xue Z, Peng Q, Chandiran AK, Liu B, et al. Mesoscopic $CH_3 NH_3 PbI_3$ /TiO_2 Heterojunction Solar Cells. J Am Chem Soc. 2012 Oct 24;134(42):17396–9.
[33] Mohammed MKA. High-performance hole conductor-free perovskite solar cell using a carbon nanotube counter electrode. RSC Adv. 2020;10(59):35831–9.
[34] Burgelman M, Decock K, Khelifi S, Abass A. Advanced electrical stimulation of thin film solar cells. Thin Solid Films. 2013 May;535:296–301.
[35] Abdulmalik MO, Danladi E, Obasi RC, Gyuk PM, Salifu FU, Magaji S, et al. Numerical Study of 25.459% Alloyed Inorganic Lead-Free Perovskite CsSnGeI3-Based Solar Cell by Device Simulation. East Eur J Phys. 2022 Dec 6;(4):125–35.
[36] Danladi E, Egbugha AC, Obasi RC, Tasie NN, Achem CU, Haruna IS, et al. Defect and doping concentration study with series and shunt resistance influence on graphene modified perovskite solar cell: A numerical investigation in SCAPS-1D framework. J Indian Chem Soc. 2023 May;100(5):101001.
[37] Kim M, Choi I woo, Choi SJ, Song JW, Mo SI, An JH, et al. Enhanced electrical properties of Li-salts doped mesoporous TiO2 in perovskite solar cells. Joule. 2021 Mar;5(3):659–72.
[38] Lee YM, Maeng I, Park J, Song M, Yun JH, Jung MC, et al. Comprehensive Understanding and Controlling the Defect Structures: An Effective Approach for Organic-Inorganic Hybrid Perovskite-Based Solar-Cell Application. Front Energy Res. 2018 Nov 29;6:128.
[39] Agresti A, Pescetelli S, Cinà L, Konios D, Kakavelakis G, Kymakis E, et al. Efficiency and Stability Enhancement in Perovskite Solar Cells by Inserting Lithium-Neutralized Graphene Oxide as Electron Transporting Layer. Adv Funct Materials. 2016 Apr;26(16):2686–94.
[40] Mohammadi S, Akbari Nia S, Abbaszadeh D. Reduction of recombination at the interface of perovskite and electron transport layer with graded pt quantum dot doping in ambient air-processed perovskite solar cell. Sci Rep. 2024 Oct 16;14(1):24254.
[41] Zhao F, Guo Y, Yang P, Tao J, Jiang J, Chu J. Effect of Li-doped TiO_2 layer on the photoelectric performance of carbon-based $CsPbIBr_2$ perovskite solar cell. J Alloys Compd. 2023 Jan;930:167377.
[42] Min H, Lee DY, Kim J, Kim G, Lee KS, Kim J, et al. Perovskite solar cells with atomically coherent interlayers on SnO_2 electrodes. Nature. 2021 Oct 21;598(7881):444–50.
[43] Mohammed MKA, Al-Mousoi AK, Kumar A, Katae ARJ, Khaleel OA, Ahmed DS, et al. Fluorinated carbon nanotubes: a low-cost hole transport layer for perovskite solar cells. J Mater Sci. 2023 Jul;58(28):11748–60.
[44] Zhang M, Chouchane M, Shojaee SA, Winiarski B, Liu Z, Li L, et al. Coupling of multiscale imaging analysis and computational modeling for understanding thick cathode degradation mechanisms. Joule. 2023 Jan;7(1):201–20.

[45] Yang T, Jeon NJ, Shin H, Shin SS, Kim YY, Seo J. Achieving Long-Term Operational Stability of Perovskite Solar Cells with a Stabilized Efficiency Exceeding 20% after 1000 h. Advanced Science. 2019 Jul;6(14):1900528.
[46] Du HJ, Wang WC, Zhu JZ. Device simulation of lead-free $CH_3NH_3SnI_3$ perovskite solar cells with high efficiency. Chinese Phys B. 2016 Oct;25(10):108802.
[47] Koh TM, Krishnamoorthy T, Yantara N, Shi C, Leong WL, Boix PP, et al. Formamidinium tin-based perovskite with low E_g for photovoltaic applications. J Mater Chem A. 2015;3(29):14996–5000.
[48] Patel PK. Device simulation of highly efficient eco-friendly $CH_3NH_3SnI_3$ perovskite solar cell. Sci Rep. 2021 Feb 4;11(1):3082.
[49] Dagar J, Castro-Hermosa S, Lucarelli G, Zampetti A, Cacialli F, Brown TM. Low-Temperature Solution-Processed Thin SnO_2/Al_2O_3 Double Electron Transport Layers Towards 20% Efficient Perovskite Solar Cells. IEEE J Photovoltaics, Sept;9(5):1309-15.
[50] Qasim I, Ahmad O, Rashid A, Zehra T, Malik MI, Rashid M, et al. Numerical optimization of (FTO/ZnO/CdS/$CH_3NH_3SnI_3$/GaAs/Au) perovskite solar cell using solar capacitance simulator with efficiency above 23% predicted. Opt Quant Electron. 2021 Dec;53(12):713.
[51] Jiao Y, Lv Y, Li J, Niu M, Yang Z. Exploring electronic and optical properties of CH 3 NH 3 GeI 3 perovskite: Insights from the first principles. Comput Theor Chem. 2017 Aug;1114:20–4.
[52] Sun PP, Chi WJ, Li ZS. Effects of water molecules on the chemical stability of $MAGeI_3$ perovskite explored from a theoretical viewpoint. Phys Chem Phys. 2016;18(35):24526–36.